University of Reading

# *ENSO modulation of MJO teleconnections to the north Atlantic & Europe*

Article

Published Version

Creative Commons: Attribution 4.0 (CC-BY)

Open access

Lee, R. W. ORCID: https://orcid.org/0000-0002-1946-5559, Woolnough, S. J. ORCID: https://orcid.org/0000-0003-0500-8514, Charlton-Perez, A. J. ORCID: https://orcid.org/0000-0001-8179-6220 and Vitart, F. (2019) ENSO modulation of MJO teleconnections to the north Atlantic & Europe. Geophysical Research Letters, 46 (22). pp. 13535-13545. ISSN 0094-8276 doi: 10.1029/2019GL084683 Available at https://centaur.reading.ac.uk/87077/

It is advisable to refer to the publisher's version if you intend to cite from the work. See Guidance on citing.

To link to this article DOI: http://dx.doi.org/10.1029/2019GL084683

Publisher: American Geophysical Union

All outputs in CentAUR are protected by Intellectual Property Rights law, including copyright law. Copyright and IPR is retained by the creators or other copyright holders. Terms and conditions for use of this material are defined in the End User Agreement.

www.reading.ac.uk/centaur

University of Reading

**CentAUR**

Central Archive at the University of Reading

Reading's research outputs online

Geophysical Research Letters

RESEARCH LETTER
10.1029/2019GL084683

# ENSO Modulation of MJO Teleconnections to the North Atlantic and Europe

R. W. Lee[1,2], S. J. Woolnough[1,2], A. J. Charlton-Perez[2], and F. Vitart[3]

[1]National Centre for Atmospheric Science, Reading, UK, [2]Department of Meteorology, University of Reading, Reading, UK, [3]European Centre for Medium-Range Weather Forecasts, Reading, UK

**Key Points:**
- There is a robust dependence of the teleconnections from the MJO to North Atlantic-European weather regimes on the phase of ENSO
- The MJO to NAO+ regime teleconnection via the troposphere is strongly enhanced during El Niño years, and suppressed during La Niña
- The MJO to NAO− regime teleconnection via the stratosphere is enhanced during La Niña years, and suppressed during El Niño

**Supporting Information:**
- Supporting Information S1

**Correspondence to:**
R. W. Lee,
r.w.lee@reading.ac.uk

**Citation:**
Lee, R. W., Woolnough, S. J., Charlton-Perez, A. J., & Vitart, F. (2019). ENSO modulation of MJO teleconnections to the North Atlantic and Europe. *Geophysical Research Letters*, *46*. https://doi.org/10.1029/2019GL084683

Received 24 JUL 2019
Accepted 29 OCT 2019

**Abstract** The teleconnection from the Madden-Julian Oscillation (MJO) provides a source of subseasonal variability and predictability to the North Atlantic-European (NAE) region. The El Niño-Southern Oscillation (ENSO) modulates the seasonal mean state, through which the MJO and its teleconnection pattern propagates; however, its impact on this teleconnection to the NAE region has not been investigated. Here we find a robust dependence of the teleconnections from the MJO to NAE weather regimes on the phase of ENSO. We show that the MJO to NAO+ regime tropospheric teleconnection is strongly enhanced during El Niño years, via enhanced Rossby wave activity, and suppressed during La Niña. Conversely, the MJO to NAO− regime stratospheric teleconnection is enhanced during La Niña years and suppressed during El Niño. This dependence on the background state has strong implications for subseasonal predictability, including interannual variations in subseasonal predictive skill.

**Plain Language Summary** The Madden-Julian Oscillation (MJO) is the dominant source of differing weather conditions in the tropics on timescales within a season. The remote linkage (teleconnection) from the MJO to the North Atlantic-European (NAE) region provides a source to modify or persist weather conditions and add predictive power to weather forecasts on 10- to 30-day timescales. The El Niño-Southern Oscillation (ENSO) has an influence on the seasonal climate state, through which the waves and linkages from the MJO to the NAE region travel. Here we find a robust dependence of these teleconnections from the MJO to NAE weather regime patterns on the ENSO state, such that under certain states of the MJO, certain regimes occur more than twice as often. The different sources and pathways also become clearer, with the teleconnections travelling via the troposphere and the stratosphere. This dependence on ENSO state has significant implications for predictions on 10- to 30-day timescales.

## 1. Introduction

Anomalous tropical meridional divergence associated with MJO (Madden & Julian, 1994) convection acts as a Rossby wave source on the subtropical jet (Seo & Lee, 2017; Seo & Son, 2012; Tseng et al., 2019). Subsequent downstream propagation and Rossby wave breaking (Franzke et al., 2004; Michel & Rivière, 2011; Swenson et al., 2017; Woollings et al., 2008) in the NAE region perturb the storm track, blocking, and jet position. This teleconnection pattern (Black et al., 2017; Cassou, 2008; Garfinkel et al., 2014; Guo et al., 2017; Henderson et al., 2016; Jiang et al., 2017; L'Heureux & Higgins, 2008; Lin et al., 2009; Moon et al., 2011; Stan et al., 2017; Vitart, 2017; Yadav & Straus, 2017) from the tropics results in a lagged and asymmetrical relationship in the NAE region. This MJO-NAE teleconnection therefore extends the potential predictability for the NAE region beyond the typical extratropical week limit into subseasonal timescales (Cassou, 2008; Tseng et al., 2018).

The lag from the MJO event to the response in the NAE region is around 10 days, but this can vary by many days, making precise attributions uncertain. The teleconnection timescale depends on differing lengths of the teleconnection pathway for different MJO phases, differing propagation speeds of MJO events yielding differing teleconnection responses (Yadav & Straus, 2017), and the NAE region simultaneously responding to multiple positions of MJO convection considering different lags (e.g. Branstator, 2014).

This influence in the NAE region may be studied by examining anomalies in weather regimes (Michelangeli et al., 1995; Neal et al., 2016; Vautard, 1990), jet regimes (Madonna et al., 2017; Woollings et al., 2010), blocking (Henderson et al., 2016), empirical orthogonal functions, or large-scale dynamical flow pattern indices, including the North Atlantic Oscillation (NAO) index (Hurrell et al., 2003). Weather regimes are commonly

©2019. American Geophysical Union. All Rights Reserved.

diagnosed using a partition algorithm to generate clusters from daily maps of geopotential height, with four regimes optimal for the NAE winter (Cassou, 2008; Michelangeli et al., 1995). Two of these are often (Cassou, 2008; Hurrell et al., 2003; Vautard, 1990) viewed as another representation of the negative and positive phases of the NAO (NAO− and NAO+, respectively). However, while the NAO+ regime closely resembles the NAO+ index, the NAO− weather regime less closely resembles the NAO− index due to a stronger contribution from the East Atlantic pattern (second empirical orthogonal function of the NAE circulation). The third regime is named Atlantic Ridge (AR), with a blocking ridge in the central North Atlantic, and the fourth is named Scandinavian Blocking (SB) with a blocked flow pattern in the North Sea region. Use of the term "blocking" in the context of weather regimes does not have any persistence criteria added. The four NAE weather regimes together describe the full range of large-scale variability of weather in the region, in contrast to the NAO index which represents 16.4% of the variance.

An MJO-lagged anomalous weather regime contingency table framework established by Cassou (2008) (comparable to Figure 1a) has shown that starting ~10 days after MJO phase 3 (active convection over the eastern Indian Ocean), the occurrence of NAO+ regime is increased by ~60% relative to climatology. This large increase extends through lags up to 12 days after MJO phase 4. This progression in the distribution is in accordance with the nominal ~6 days between each of the numbered MJO phases. Next, there appears a small (~30%) enhanced occurrence of SB and AR regimes at lags of around 0–6 and 10 days, respectively, likely as a result of in situ development. That is, the response to the MJO initiated the NAO+ regime, but the subsequent evolution emerges following internal dynamics in the NAE region independent of MJO forcing. For lags greater than 10 days after MJO phase 6 (active convection over the western Pacific Ocean) NAO− builds up to ~70% increased occurrence and lasts through MJO phase 8. When the occurrence of NAO+ is increased, the other regimes decrease (in particular NAO−), and vice versa.

Finally, the phase of ENSO provides a seasonal mean teleconnection to the NAO, being strongest between (moderate) El Niño and NAO− (Li & Lau, 2012; Toniazzo & Scaife, 2006), proving robust between Central Pacific, and Eastern Pacific El Niño events (Zhang et al., 2018). Viewed from the subseasonal perspective however, ENSO modulates the global background state, through which the MJO and its subseasonal teleconnection pattern propagates (Moon et al., 2011; Roundy et al., 2010; Son et al., 2017). For example, larger MJO-related subseasonal variability extends further east in the Pacific during El Niño years (e.g. Hendon et al., 1999). An ENSO phase dependency is apparent in the MJO teleconnection to the North Pacific Rim, seen in the Pacific storm track activity (Takahashi & Shirooka, 2014), and large-scale circulation over North America (Moon et al., 2011). The magnitude of the MJO influence on the NAO index was suggested to have an ENSO phase dependency, with this modulation greatest during La Niña conditions or during periods of rapid ENSO adjustment (Roundy et al., 2010). It is important to consider feedback between ENSO (and its associated midlatitude background state) and intraseasonal variability including the MJO since their existence modifies seasonal ENSO response (Swenson & Straus, 2015), implying the potential for rectification.

Here we investigate the dependence of the extended boreal winter (November–March) subseasonal MJO-NAE teleconnection on the interannual variations in the background state associated with ENSO and find the dependence robust. A better understanding of this is important for assessing the representation of this dependence in weather and climate models and improving predictions.

We use the RMM index to describe the MJO phase (Text S1 in the supporting information) (Wheeler & Hendon, 2004), the NAE weather regimes (Text S2), and the Cassou (2008) contingency table framework (Text S3), updated with the ERA-Interim reanalysis (Dee et al., 2011) over 1979–2018. We find that the overall MJO-NAE weather regime teleconnections are very similar (Figure 1a) to the original study (Cassou, 2008), with two minor differences. First, the increased occurrence of NAO+ seen 10 days after MJO phase 3 now appears significant earlier, after MJO phase 1. Secondly, the increased AR and SB regime occurrences after MJO phases 4–6. These differences are likely due to a longer data period, adding to the sample size, and a different dataset.

## 2. Impact of ENSO Background State

In order to examine the ENSO modulation of these MJO-NAE teleconnections, we build on the Cassou framework by using an index created from the annual winter mean Niño3.4 sea surface temperature

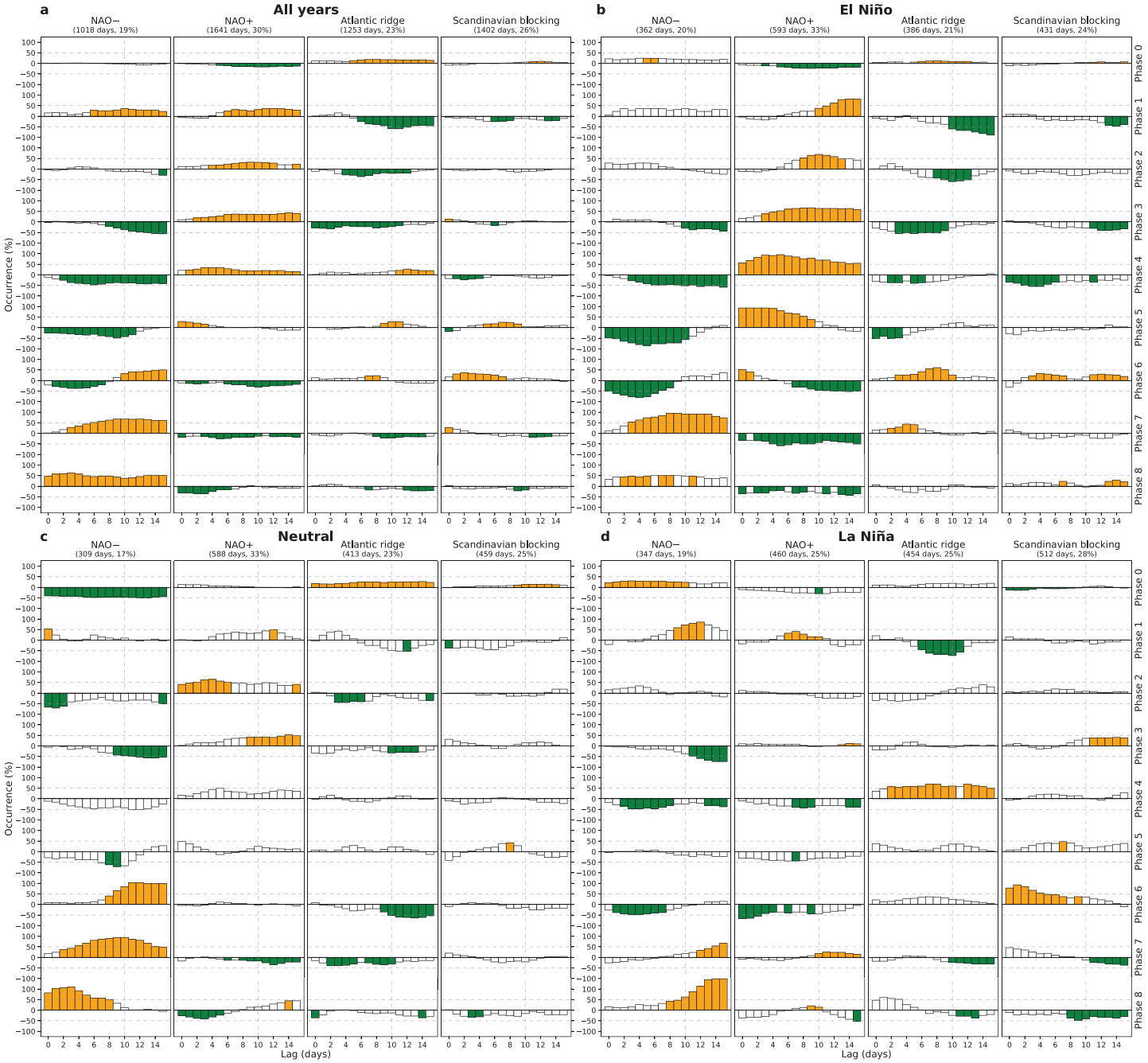


**Figure 1.** ENSO modulates MJO teleconnections shown by frequency anomalies. Table of contingency (Text S3) between the MJO phases (rows) and the NAE weather regimes (columns) composited over (a) all, (b) El Niño, (c) neutral, and (d) La Niña extended winters. For each MJO phase, we plot the anomalous percentage occurrence of a given regime as a function of lag in days (with regimes lagging MJO phases). The orange and green bars show where the regimes occur significantly more or less frequently, respectively, than their climatological occurrences.

(SST) (Rayner, 2003) (Text S4). This index is then split into terciles to composite the data, which are termed "years." During El Niño years (Figure 1b), the NAO+ teleconnection is of a much larger amplitude, significant following MJO phase 1, with increased occurrence up to ~100% (twice climatology), restoring to climatology around 6 days (one MJO phase) later. When there is no active MJO teleconnection (phase 0; around one third of winter days), there is an increased frequency of NAO− and AR, and decreased frequency of NAO+. However, when including the MJO active days, the

change in the overall distribution between the weather regimes during El Niño years is a 3 percentage point increase in NAO+ days relative to all years and a 2 percentage point decrease in AR days, due to the strong MJO-NAO+ teleconnection, suggesting that there may be a rectification onto the seasonal mean state. The AR and SB regimes follow, with increases up to 50% after MJO phase 6, associated with the in situ development from NAO+. The NAO− regime has significant increases in occurrence only after MJO phase 7 (also up to ~100%). This rapid shift from AR and SB may be suggestive of in situ development rather than a full MJO teleconnection. We therefore conclude that the MJO-NAE teleconnection during El Niño years results in a much more frequent NAO+ regime state, occurring after MJO phases 1–5 and dominating the seasonal mean teleconnection.

During neutral years (Figure 1c), the NAO+ teleconnection is similar to the all-years teleconnection, with amplitudes half that of El Niño years; however with a reduced sample size much of it is not significant. Without a strong NAO+ teleconnection there appears to be no evidence of in situ development to AR or SB regimes. AR occurs ~25% more often when no MJO is active during neutral years. The most important difference is the active NAO− teleconnection, after MJO phase 6, with amplitudes up to 100% increased occurrence, through to phase 8. With no active MJO there are approximately 50% fewer occurrences of NAO−, and despite the strong teleconnection, its short duration (only two MJO phases) means that it does not restore the neutral mean NAO− (17% of all days) up to the level of all years (19% of all days). We conclude that the MJO-NAE teleconnection during neutral years results in a slightly more frequent NAO+ state after MJO phases 1–4, and a much more frequent NAO− regime state, occurring after MJO phases 6–7.

La Niña years (Figure 1d) show no NAO+ teleconnection, while the large NAO− teleconnection is later in the MJO phase cycle (beyond MJO phase 8) and fades before reaching lag day 0 (at what would be MJO phase 2). During the extended winter under La Niña conditions, there are fewer occurrences of long lived MJO episodes that last through multiple phases following phase 8, compared to the other ENSO states (Figure S1 in the supporting information). This implies that those events in the contingency table during phase 2 are often new events and therefore lose the teleconnection anomaly triggered in phase 8 only as a result of this analysis framework. AR and SB have increased occurrences after MJO phases 4 and 6, respectively, and are most likely related to in situ development. We conclude that the only complete MJO-NAE teleconnection during La Niña years is a strong NAO− teleconnection, occurring around 1.5 MJO phases later than the neutral years equivalent.

ENSO modulation of the spatial distribution and strength of MJO teleconnections generally agree with the frequency anomalies (Figure 1), focusing on the third pentad lag from the MJO (Figure 2). The clear NAO+ regime pattern follows phases 1–4 during El Niño years (but not in the seasonal mean teleconnection), and in neutral years this signal is only apparent after phase 3. Similarly, the AR pattern following SB, after MJO phases 4 and 3, respectively, during La Niña years is also apparent in the spatial distributions. The NAO− teleconnection shows up during neutral years after MJO phases 6 but the spatial pattern shifts north, and by phase 7 it is almost entirely dominated by the negative lobe of the pattern. During El Niño years after phases 6–8 the negative lobe of NAO− is also much larger than the positive lobe, and phase 8 during La Niña years also links to a northward offset of the NAO− regime pattern. The result of averaging El Niño, neutral, and La Niña groups together to make "all years" for each MJO phase is apparent, with the strongest anomalies contributing most.

## 3. Modulation of Wave Propagation

Weather regime development is dynamically linked with Rossby wave breaking (Swenson et al., 2017), and high- and low-frequency wave trains from upstream (Feldstein, 2003; Franzke et al., 2004). The NAO− is almost entirely related to cyclonic wave breaking (CWB) (Rivière & Orlanski, 2007; Swenson et al., 2017) on the poleward side of the climatological jet, developing from an in situ single wave breaking event (Franzke et al., 2004). SB and AR are directly coincident with anticyclonic wave breaking (AWB) (Swenson et al., 2017). NAO+ is strongly linked to multiple AWB events, initially upstream over the Pacific, and then following a low-frequency mid-latitude anomalous wave train, a further AWB in the eastern Atlantic on the equatorward side of the climatological jet, likely through downstream development (Benedict et al., 2004; Feldstein, 2003; Franzke et al., 2004; Rivière & Orlanski, 2007; Swenson et al.,

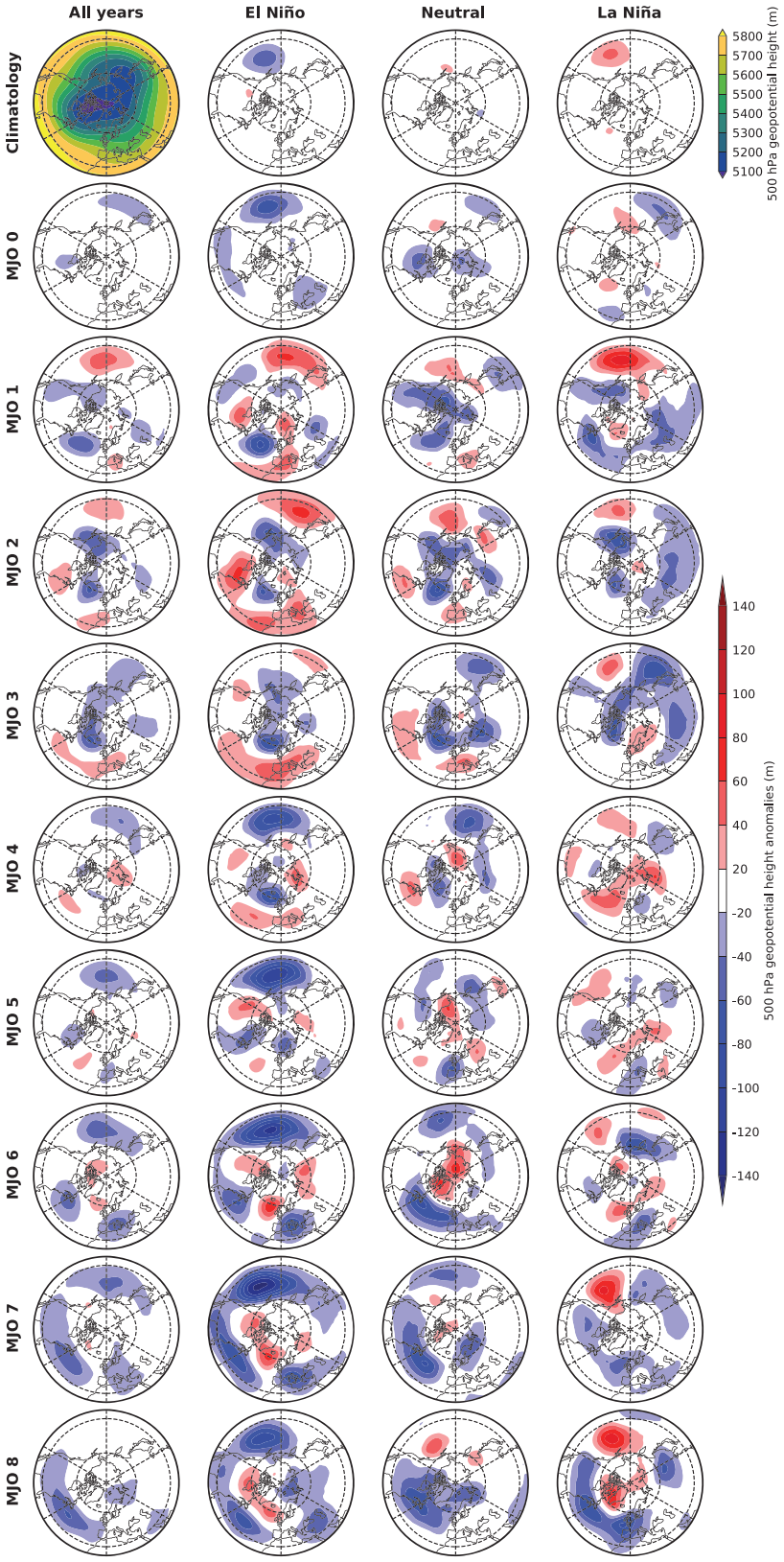


**Figure 2.** ENSO modulates MJO teleconnections shown by circulation amplitude anomalies. About 500 hPa geopotential height anomalies composited for the full climatology and seasonal anomalies (top row), and the third pentad mean from MJO phases 0–8 (other rows). Anomalies are relative to the "all years" seasonal cycle. Shown north of the Tropic of Cancer, gridlines at 30°N, 60°N and every 60° longitude.

2017). Lagged geopotential height composites show the low-frequency wave train from the eastern Pacific to the NAE, present following MJO phase 3 (Figure 3a) but not phase 6 (Cassou, 2008). Splitting this MJO phase 3 lagged composite by ENSO state reveals important differences in this forcing. This wave train is only present during El Niño and neutral years; there is no clear wave train during La Niña years. With no wave train there are not sufficient conditions for AWB, explaining why there is no NAO+ teleconnection during La Niña years. The strongest wave train anomalies occur during El Niño years, also in agreement with the more frequent and stronger NAO+ anomalies following MJO phase 3 (Figures 1 and 2).

Upstream there are clear differences in the positions of the upper level jets after MJO phase 3 (Figure 3b), with the exit of the Pacific jet in close proximity to the entrance of the Atlantic jet during El Niño years. During La Niña years the Pacific jet exit is located further northwest of the Atlantic jet entrance. Further upstream, in the main Rossby wave source region, the location and longitudinal width of the MJO convection has been shown to be important in the triggering of Rossby waves (Seo et al., 2016; Seo & Lee, 2017; Tseng et al., 2019). The anomalous divergent wind north of the convection induces two major Rossby wave source regions on the subtropical jet around southern Asia and the western North Pacific, with the dividing axis over the east Asian coast. When these two Rossby wave source regions are trigged in an asymmetric dipole-like pattern, the constructive interference induces a stronger Rossby wave train and teleconnection downstream. Conversely, where the pattern is instead symmetric (a monopole) about the axis, destructive interference reduces the Rossby wave train. Forcing with zonal wave numbers 1 and 2 propagates Rossby waves in direct arclike canonical pattern, while it is only the shorter waves, which propagate along the jet, acting as a waveguide (Hoskins & Ambrizzi, 1993; Seo et al., 2016; Seo & Lee, 2017). Rossby wave pathways can be inferred from horizontal wave activity flux (Figure 3b and Text S6) (Takaya & Nakamura, 2001), with the group velocity of a stationary Rossby wave being approximately parallel to these vectors; their divergence indicating a Rossby wave source and convergence implies a Rossby wave absorption/sink. During MJO phase 3 in El Niño years, enhanced wave activity develops within the subtropical jet in response to the asymmetric dipole of enhanced and suppressed convection. The anomalous Walker circulation, enhanced by El Niño, acts to shorten the wavelength of these convective dipoles, leading to an optimal Rossby wavenumber (>3) generation for jet to act as a waveguide. With the Pacific and Atlantic jets closely aligned, this enhanced wave train then, at later lags (not shown), reaches the NAE region where the waves then break (AWB) triggering the NAO+ regime. Whereas during MJO phase 3 in La Niña years the dipole of the total convection is now much broader in its zonal extent, which does not create the forcing dipole over east Asian jet region and only forces large wavelength Rossby waves (<3), and weaker circulation anomalies. This reduces the strength of the wave activity along most of the Pacific and Atlantic jets, with the exception of the northeast North Pacific (where there is a more local wave activity source and sink with fewer waves not entering the Atlantic jet).

Besides the 10- to 15-day tropospheric pathway from the MJO to the NAE region, there is also a subseasonal stratospheric pathway. The state of the stratospheric polar vortex has a clear impact on the NAE (Scaife et al., 2005) weather regimes (Charlton-Perez et al., 2018). NAO− is most sensitive to this stratospheric state, occurring on 33% of days following weak vortex conditions but on only 5% of days following strong vortex conditions, while an opposite and slightly weaker sensitivity is found for NAO+ and AR (Charlton-Perez et al., 2018). The pathway from the MJO to the stratosphere is primarily driven by poleward and vertical Rossby wave propagation (Garfinkel et al., 2012, 2014). After MJO phase 7 a low develops in the North Pacific, leading to more heat flux, establishing warm anomalies in the polar lower stratosphere and a weakened stratospheric polar vortex. In contrast, phase 3 leads to the opposite effects: anomalous cooling in the stratosphere and a strengthened polar vortex. We find that the MJO–polar vortex–NAE pathway is strongly active during La Niña years (Figure 3c), particularly for the weakened vortex following MJO phases 8 (corresponding to the third pentad after phases 6–7 in Figure 2), associated with the low in the northwest Pacific following MJO phase 7, increasing vertical heat flux to the stratosphere. There is also a weakened vortex closely following MJO phases 7–8 during neutral years. These contribute to the increased NAO− occurrence around phases 7–8 during neutral and La Niña years (Figure 1). The increased vortex strength following MJO phases 2–3 (Figure 3c) provides a link to the enhanced prevalence of the AR (Figure 1) after MJO phase 4 during La Niña years.

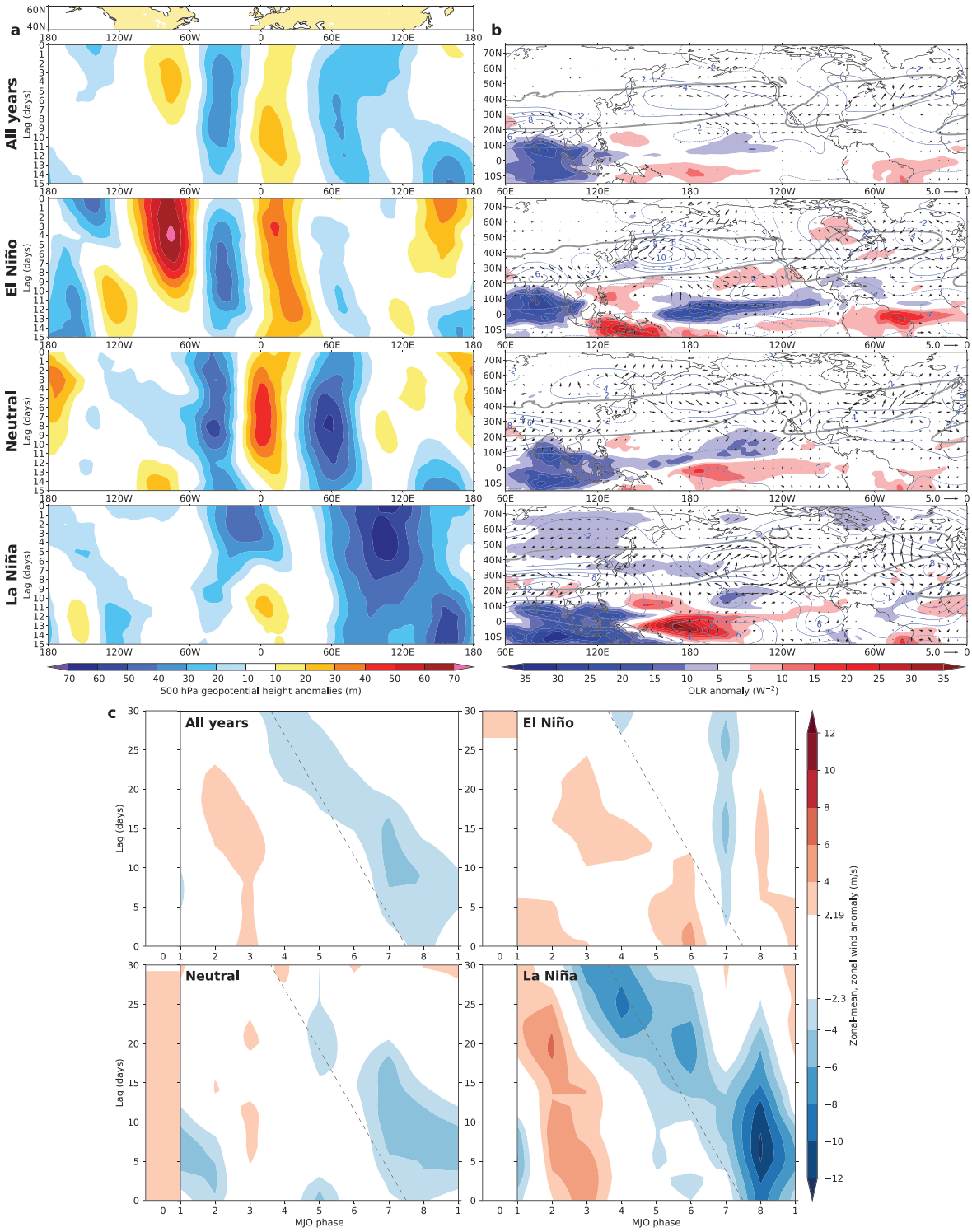


**Figure 3.** ENSO modulates MJO phase 3 tropospheric Rossby wave propagation, wave source and flux, and alignment between the Pacific and Atlantic jets, and modulates the stratospheric polar vortex strength response to the MJO. (a) 500 hPa geopotential height anomalies (40–60°N), composited as a Hovmöller from MJO phase 3. (b) 300 hPa zonal wind isotach (grey thick contour showing 22 m $s^{-1}$), streamfunction anomalies (blue contours, intervals $2 \times 10^{-6}$ $m^2$ $s^{-1}$, zero contour suppressed), phase-independent wave-activity flux anomalies (vectors, scale shows 5 $m^2$ $s^{-2}$, anomalies below 0.5 $m^2$ $s^{-2}$ are suppressed; Text S6), and Outgoing Longwave Radiation anomalies (color shading), composited as the first pentad after MJO phase 3. (c) The stratospheric polar vortex strength (zonal wind at 60°N at 100 hPa) response to each MJO phase, and without an active MJO (phase 0; left column in each panel). The dashed line indicates the approximate progression of a constant MJO state as a function of lag. Values of vortex strength which do not have a significant impact on the NAE weather regimes are uncolored using thresholds calculated from a first-order Markov model (Charlton-Perez et al., 2018). For all panels, anomalies are relative to the "all years" seasonal cycle.

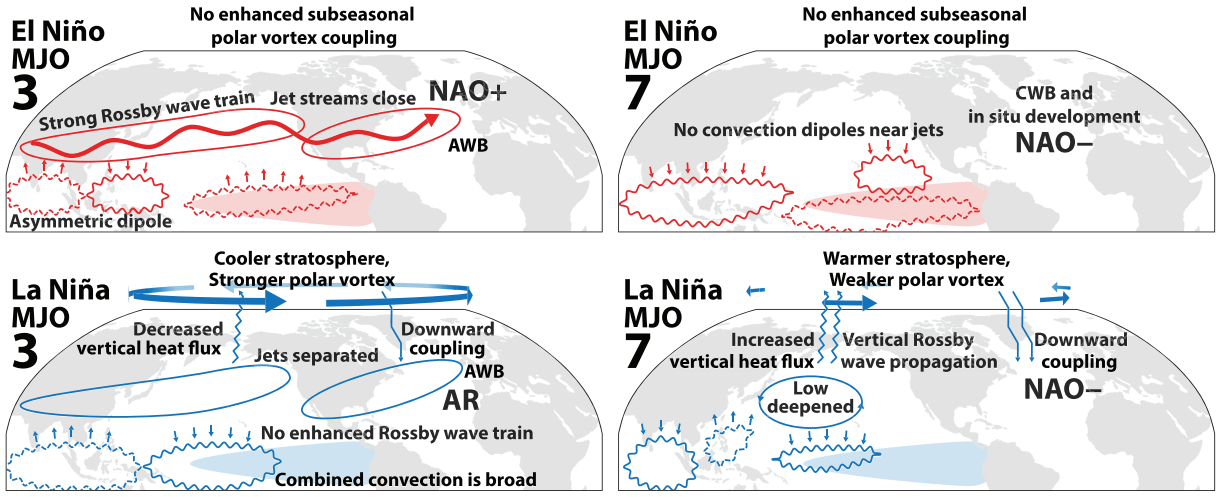


**Figure 4.** Schematic of ENSO modulation of subseasonal teleconnections from the MJO to the NAE region (narrative: Text S7). El Niño (upper panels; red) and La Niña (lower panels; blue) states are illustrated following MJO phases 3 (left panels) and 7 (right panels). AWB and CWB refer to anticyclonic wave breaking, and cyclonic wave breaking, respectively. The anomalous convection signals (solid: enhanced; dashed: suppressed) comprise the MJO, in the given phases, as modified by the large-scale ENSO circulation.

Teleconnections on longer timescales modulate the MJO-NAE subseasonal teleconnection by dynamically changing the background state. There is an association between the MJO and the stratospheric quasi-biennial oscillation (QBO), which has a strong control on MJO activity (Son et al., 2017), propagation (Densmore et al., 2019; Hendon & Abhik, 2018; Son et al., 2017), amplitude (Densmore et al., 2019; Klotzbach et al., 2019), and persistence (Lim et al., 2019), leading to higher MJO prediction skill during easterly QBO winters (Lim et al., 2019). Further research is needed to investigate the impacts of the QBO background state on the ENSO modulation of the MJO-NAE subseasonal teleconnection.

The seasonal ENSO-NAO teleconnection is both via the stratosphere and troposphere in tandem (Jiménez-Esteve & Domeisen, 2018); however, both follow very similar mechanisms to those on subseasonal timescales (Garfinkel et al., 2012, 2014). Seasonal stratospheric mechanisms (Jiménez-Esteve & Domeisen, 2018; Toniazzo & Scaife, 2006) focus on modifying the amplitude of extratropical stationary waves (Hamilton, 1993), and stratospheric polar vortex strength (Domeisen et al., 2019; Sassi et al., 2004), while tropospheric mechanisms (Jiménez-Esteve & Domeisen, 2018; Li & Lau, 2012) also modify the intensity of transient disturbances and the latitude and speed of the North Pacific jet and its proximity to the Atlantic jet.

## 4. Discussion

Our findings demonstrate that the subseasonal teleconnections from the MJO to the NAE weather regimes are strongly dependent on the ENSO background state (summary schematic: Figure 4). The NAO+ regime tropospheric teleconnection from MJO phases 1–5 is strongly enhanced during El Niño years, persisting throughout more MJO phases, while it is suppressed during La Niña years. The NAO − regime teleconnection via the stratosphere from MJO phases 7–8 is most enhanced and occurring latest during La Niña years, while it is suppressed during El Niño years. Neutral years feature aspects of both of these teleconnections. NAE regime progression, in situ development, and the differing dynamical teleconnection mechanisms also become clearer via this perspective separated by ENSO state. The ENSO circulation anomaly modifies the MJO convection, impacting the Rossby waves generated, and their teleconnection pathways to the NAE region.

The changes in the weather regime distributions present evidence of the rectification of subseasonal teleconnections onto the seasonal mean. This rectification implies that it is important to have a good representation of this subseasonal teleconnection in any general circulation model used to study climate states and their interactions.

The dependence of the teleconnections on the background state suggests a potential sensitivity of the MJO-NAE teleconnections to climate change, in particular any change in ENSO, tropospheric jets, and the stratospheric polar vortex. The dependence on the background state also has strong implications for subseasonal predictability, including interannual variations in subseasonal predictive skill. For example, the increased likelihood of NAO+ following MJO phases 1–5 in El Niño years suggests that the NAO+ regime is likely to be more predictable during El Niño years since this teleconnection is stronger. This would apply to the predictability of the climate system, and the predictive skill in subseasonal numerical models, which can accurately represent these processes. This also stresses the importance for models to get the background state correct to represent these teleconnections, in addition to having sufficient skill at representing the MJO. Thus, it may be that errors in the teleconnection of MJO-NAE region are related to errors in the background state, which may include model representation of the ENSO-MJO interaction, the seasonally evolving mean state, and ENSO seasonal teleconnections. Finally, we note that if these teleconnections are then too weak, they may then contribute to the so-called "signal-to-noise paradox" (Scaife & Smith, 2018) seen in seasonal prediction models (Dunstone et al., 2016; Scaife et al., 2014) via a lack of weather regime persistence (Strommen & Palmer, 2019).

**Acknowledgments**
This work is supported by the InterDec project, funded by NERC grant NE/P00678/1, originating from the 2015 call from the Belmont Forum and JPI-Climate for collaborative research action. S. J. W. is also supported by the National Centre for Atmospheric Science, a NERC collaborative centre under contract R8/H12/83/001. We thank the European Centre for Medium Range Weather Forecasting (ECMWF) for use of the ECMWF Interim Reanalysis (ERA-Interim) data, obtained from the ECMWF data server. We thank Matt Wheeler for the RMMI data. We thank the two anonymous reviewers for their constructive comments. Data related to this paper can be downloaded from the following: RMMI, http://poama.bom.gov.au/project/maproom/RMM/createdPCs.TotAnom.74toRealtime.txt; ERA-Interim, https://apps.ecmwf.int/datasets/data/interim-full-daily/levtype=pl/; and Niño 3.4 SST Index (calculated from HadISST1), https://www.esrl.noaa.gov/psd/gcos_wgsp/Timeseries/Data/nino34.long.anom.data. The analyses were performed using Python.

## References

Benedict, J. J., Lee, S., & Feldstein, S. B. (2004). Synoptic view of the North Atlantic Oscillation. *Journal of the Atmospheric Sciences*, *61*(2), 121–144. https://doi.org/10.1175/1520-0469(2004)061<0121:SVOTNA>2.0.CO;2

Black, J., Johnson, N. C., Baxter, S., Feldstein, S. B., Harnos, D. S., & L'Heureux, M. L. (2017). The predictors and forecast skill of Northern Hemisphere teleconnection patterns for lead times of 3–4 weeks. *Monthly Weather Review*, *145*(7), 2855–2877. https://doi.org/10.1175/MWR-D-16-0394.1

Branstator, G. (2014). Long-lived response of the midlatitude circulation and storm tracks to pulses of tropical heating. *Journal of Climate*, *27*(23), 8809–8826. https://doi.org/10.1175/JCLI-D-14-00312.1

Cassou, C. (2008). Intraseasonal interaction between the Madden–Julian Oscillation and the North Atlantic Oscillation. *Nature*, *455*(7212), 523–527. https://doi.org/10.1038/nature07286

Charlton-Perez, A. J., Ferranti, L., & Lee, R. W. (2018). The influence of the stratospheric state on North Atlantic weather regimes. *Quarterly Journal of the Royal Meteorological Society*, *144*(713), 1140–1151. https://doi.org/10.1002/qj.3280

Dee, D. P., Uppala, S. M., Simmons, A. J., Berrisford, P., Poli, P., Kobayashi, S., et al. (2011). The ERA-Interim reanalysis: Configuration and performance of the data assimilation system. *Quarterly Journal of the Royal Meteorological Society*, *137*(656), 553–597. https://doi.org/10.1002/qj.828

Densmore, C. R., Sanabia, E. R., & Barrett, B. S. (2019). QBO influence on MJO amplitude over the Maritime Continent: Physical mechanisms and seasonality. *Monthly Weather Review*, *147*(1), 389–406. https://doi.org/10.1175/MWR-D-18-0158.1

Domeisen, D. I. V., Garfinkel, C. I., & Butler, A. H. (2019). The teleconnection of El Niño Southern Oscillation to the stratosphere. *Reviews of Geophysics*, *57*, 5–47. https://doi.org/10.1029/2018RG000596

Dunstone, N., Smith, D., Scaife, A., Hermanson, L., Eade, R., Robinson, N., et al. (2016). Skilful predictions of the winter North Atlantic Oscillation one year ahead. *Nature Geoscience*, *9*(11), 809–814. https://doi.org/10.1038/ngeo2824

Feldstein, S. B. (2003). The dynamics of NAO teleconnection pattern growth and decay. *Quarterly Journal of the Royal Meteorological Society*, *129*(589), 901–924. https://doi.org/10.1256/qj.02.76

Franzke, C., Lee, S., & Feldstein, S. B. (2004). Is the North Atlantic Oscillation a breaking wave? *Journal of the Atmospheric Sciences*, *61*(2), 145–160. https://doi.org/10.1175/1520-0469(2004)061<0145:ITNAOA>2.0.CO;2

Garfinkel, C. I., Benedict, J. J., & Maloney, E. D. (2014). Impact of the MJO on the boreal winter extratropical circulation. *Geophysical Research Letters*, *41*, 6055–6062. https://doi.org/10.1002/2014GL061094

Garfinkel, C. I., Feldstein, S. B., Waugh, D. W., Yoo, C., & Lee, S. (2012). Observed connection between stratospheric sudden warmings and the Madden-Julian Oscillation. *Geophysical Research Letters*, *39*, L18807. https://doi.org/10.1029/2012GL053144

Guo, Y., Shinoda, T., Lin, J., & Chang, E. K. M. (2017). Variations of Northern Hemisphere storm track and extratropical cyclone activity associated with the Madden-Julian oscillation. *Journal of Climate*, *30*(13), 4799–4818. https://doi.org/10.1175/JCLI-D-16-0513.1

Hamilton, K. (1993). An examination of observed southern oscillation effects in the Northern Hemisphere stratosphere. *Journal of the Atmospheric Sciences*, *50*(20), 3468–3474. https://doi.org/10.1175/1520-0469(1993)050<3468:AEOOSO>2.0.CO;2

Henderson, S. A., Maloney, E. D., & Barnes, E. A. (2016). The influence of the Madden-Julian oscillation on Northern Hemisphere winter blocking. *Journal of Climate*, *29*(12), 4597–4616. https://doi.org/10.1175/JCLI-D-15-0502.1

Hendon, H. H., & Abhik, S. (2018). Differences in vertical structure of the Madden-Julian Oscillation associated with the quasi-biennial oscillation. *Geophysical Research Letters*, *45*, 4419–4428. https://doi.org/10.1029/2018GL077207

Hendon, H. H., Zhang, C., & Glick, J. D. (1999). Interannual variation of the Madden–Julian Oscillation during austral summer. *Journal of Climate*, *12*(8), 2538–2550. https://doi.org/10.1175/1520-0442(1999)012<2538:IVOTMJ>2.0.CO;2

Hoskins, B. J., & Ambrizzi, T. (1993). Rossby wave propagation on a realistic longitudinally varying flow. *Journal of the Atmospheric Sciences*, *50*(12), 1661–1671. https://doi.org/10.1175/1520-0469(1993)050<1661:RWPOAR>2.0.CO;2

Hurrell, J. W., Kushnir, Y., Ottersen, G., & Visbeck, M. (2003). An overview of the North Atlantic Oscillation. In J. W. Hurrell, Y. Kushnir, G. Ottersen, & M. Visbeck (Eds.), *The North Atlantic Oscillation: Climatic significance and environmental impact*, (Vol. 134, pp. 1–35). Washington, D. C.: American Geophysical Union. https://doi.org/10.1029/GM134

Jiang, Z., Feldstein, S. B., & Lee, S. (2017). The relationship between the Madden-Julian Oscillation and the North Atlantic Oscillation. *Quarterly Journal of the Royal Meteorological Society*, *143*(702), 240–250. https://doi.org/10.1002/qj.2917

Jiménez-Esteve, B., & Domeisen, D. I. V. (2018). The tropospheric pathway of the ENSO–North Atlantic Teleconnection. *Journal of Climate*, *31*(11), 4563–4584. https://doi.org/10.1175/JCLI-D-17-0716.1

Klotzbach, P., Abhik, S., Hendon, H. H., Bell, M., Lucas, C., Marshall, G., & A., & Oliver, E. C. J. (2019). On the emerging relationship between the stratospheric Quasi-Biennial oscillation and the Madden-Julian oscillation. *Scientific Reports*, *9*(1), 1–9. https://doi.org/10.1038/s41598-019-40034-6

L'Heureux, M. L., & Higgins, R. W. (2008). Boreal winter links between the Madden–Julian Oscillation and the Arctic Oscillation. *Journal of Climate*, *21*(12), 3040–3050. https://doi.org/10.1175/2007JCLI1955.1

Li, Y., & Lau, N. C. (2012). Impact of ENSO on the atmospheric variability over the North Atlantic in late Winter-Role of transient eddies. *Journal of Climate*, *25*(1), 320–342. https://doi.org/10.1175/JCLI-D-11-00037.1

Lim, Y., Son, S.-W., Marshall, A. G., Hendon, H. H., & Seo, K.-H. (2019). Influence of the QBO on MJO prediction skill in the subseasonal-to-seasonal prediction models. *Climate Dynamics*, *53*(3–4), 1681–1695. https://doi.org/10.1007/s00382-019-04719-y

Lin, H., Brunet, G., & Derome, J. (2009). An observed connection between the North Atlantic Oscillation and the Madden–Julian Oscillation. *Journal of Climate*, *22*(2), 364–380. https://doi.org/10.1175/2008JCLI2515.1

Madden, R. A., & Julian, P. R. (1994). Observations of the 40–50-day tropical oscillation—A review. *Monthly Weather Review*, *122*(5), 814–837. https://doi.org/10.1175/1520-0493(1994)122<0814:OOTDTO>2.0.CO;2

Madonna, E., Li, C., Grams, C. M., & Woollings, T. (2017). The link between eddy-driven jet variability and weather regimes in the North Atlantic-European sector. *Quarterly Journal of the Royal Meteorological Society*, *143*(708), 2960–2972. https://doi.org/10.1002/qj.3155

Michel, C., & Rivière, G. (2011). The link between Rossby wave breakings and weather regime transitions. *Journal of the Atmospheric Sciences*, *68*(8), 1730–1748. https://doi.org/10.1175/2011JAS3635.1

Michelangeli, P.-A., Vautard, R., & Legras, B. (1995). Weather regimes: Recurrence and quasi stationarity. *Journal of the Atmospheric Sciences*, *52*(8), 1237–1256. https://doi.org/10.1175/1520-0469(1995)052<1237:WRRAQS>2.0.CO;2

Moon, J. Y., Wang, B., & Ha, K. J. (2011). ENSO regulation of MJO teleconnection. *Climate Dynamics*, *37*(5), 1133–1149. https://doi.org/10.1007/s00382-010-0902-3

Neal, R., Fereday, D., Crocker, R., & Comer, R. E. (2016). A flexible approach to defining weather patterns and their application in weather forecasting over Europe. *Meteorological Applications*, *23*(3), 389–400. https://doi.org/10.1002/met.1563

Rayner, N. A. (2003). Global analyses of sea surface temperature, sea ice, and night marine air temperature since the late nineteenth century. *Journal of Geophysical Research*, *108*(D14), 4407. https://doi.org/10.1029/2002JD002670

Rivière, G., & Orlanski, I. (2007). Characteristics of the Atlantic Storm-Track Eddy Activity and Its Relation with the North Atlantic Oscillation. *Journal of the Atmospheric Sciences*, *64*(2), 241–266. https://doi.org/10.1175/jas3850.1

Roundy, P. E., MacRitchie, K., Asuma, J., & Melino, T. (2010). Modulation of the global atmospheric circulation by combined activity in the Madden–Julian Oscillation and the El Niño–Southern Oscillation during Boreal Winter. *Journal of Climate*, *23*(15), 4045–4059. https://doi.org/10.1175/2010JCLI3446.1

Sassi, F., Kinnison, D., Bouville, B. A., Garcia, R. R., & Roble, R. (2004). Effect of El Niño–Southern Oscillation on the dynamical, thermal, and chemical structure of the middle atmosphere. *Journal of Geophysical Research*, *109*, D17108. https://doi.org/10.1029/2003JD004434

Scaife, A. A., Arribas, A., Blockley, E., Brookshaw, A., Clark, R. T., Dunstone, N., et al. (2014). Skillful long-range prediction of European and North American winters. *Geophysical Research Letters*, *41*, 2514–2519. https://doi.org/10.1002/2014GL059637

Scaife, A. A., Knight, J. R., Vallis, G. K., & Folland, C. K. (2005). A stratospheric influence on the winter NAO and North Atlantic surface climate. *Geophysical Research Letters*, *32*, L18715. https://doi.org/10.1029/2005GL023226

Scaife, A. A., & Smith, D. (2018). A signal-to-noise paradox in climate science. *npj Climate and Atmospheric Science*, *1*(28). https://doi.org/10.1038/s41612-018-0038-4

Seo, K.-H., & Lee, H.-J. (2017). Mechanisms for a PNA-like teleconnection pattern in response to the MJO. *Journal of the Atmospheric Sciences*, *74*(6), 1767–1781. https://doi.org/10.1175/JAS-D-16-0343.1

Seo, K.-H., Lee, H.-J., & Frierson, D. M. W. (2016). Unraveling the teleconnection mechanisms that induce wintertime temperature anomalies over the Northern Hemisphere continents in response to the MJO. *Journal of the Atmospheric Sciences*, *73*(9), 3557–3571. https://doi.org/10.1175/JAS-D-16-0036.1

Seo, K.-H., & Son, S.-W. (2012). The global atmospheric circulation response to tropical diabatic heating associated with the Madden–Julian Oscillation during Northern Winter. *Journal of the Atmospheric Sciences*, *69*(1), 79–96. https://doi.org/10.1175/2011JAS3686.1

Son, S.-W., Lim, Y., Yoo, C., Hendon, H. H., & Kim, J. (2017). Stratospheric control of the Madden–Julian Oscillation. *Journal of Climate*, *30*(6), 1909–1922. https://doi.org/10.1175/JCLI-D-16-0620.1

Stan, C., Straus, D. M., Frederiksen, J. S., Lin, H., Maloney, E. D., & Schumacher, C. (2017). Review of tropical-extratropical teleconnections on intraseasonal time scales. *Reviews of Geophysics*, *55*, 902–937. https://doi.org/10.1002/2016RG000538

Strommen, K., & Palmer, T. N. (2019). Signal and noise in regime systems: A hypothesis on the predictability of the North Atlantic Oscillation. *Quarterly Journal of the Royal Meteorological Society*, *145*(718), 147–163. https://doi.org/10.1002/qj.3414

Swenson, E. T., & Straus, D. M. (2015). Transient tropical diabatic heating and the seasonal-mean response to ENSO. *Journal of the Atmospheric Sciences*, *72*(5), 1891–1907. https://doi.org/10.1175/JAS-D-14-0162.1

Swenson, E. T., Straus, D. M., Swenson, E. T., & Straus, D. M. (2017). Rossby wave breaking and transient eddy forcing during Euro-Atlantic circulation regimes. *Journal of the Atmospheric Sciences*, *74*(6), 1735–1755. https://doi.org/10.1175/JAS-D-16-0263.1

Takahashi, C., & Shirooka, R. (2014). Storm track activity over the North Pacific associated with the Madden-Julian Oscillation under ENSO conditions during boreal winter. *Journal of Geophysical Research: Atmospheres*, *119*, 10,663–10,683. https://doi.org/10.1002/2014JD021973

Takaya, K., & Nakamura, H. (2001). A formulation of a phase-independent wave-activity flux for stationary and migratory quasigeostrophic eddies on a zonally varying basic flow. *Journal of the Atmospheric Sciences*, *58*(6), 608–627. https://doi.org/10.1175/1520-0469(2001)058<0608:AFOAPI>2.0.CO;2

Toniazzo, T., & Scaife, A. A. (2006). The influence of ENSO on winter North Atlantic climate. *Geophysical Research Letters*, *33*, L24704. https://doi.org/10.1029/2006GL027881

Tseng, K.-C., Barnes, E. A., & Maloney, E. D. (2018). Prediction of the midlatitude response to strong Madden-Julian Oscillation events on S2S time scales. *Geophysical Research Letters*, *45*, 463–470. https://doi.org/10.1002/2017GL075734

Tseng, K.-C., Maloney, E., & Barnes, E. (2019). The Consistency of MJO teleconnection patterns: An midlatitude response to strong. *Journal of Climate*, *32*(2), 531–548. https://doi.org/10.1175/JCLI-D-18-0211.1

Vautard, R. (1990). Multiple weather regimes over the North Atlantic: Analysis of precursors and successors. *Monthly Weather Review*, *118*(10), 2056–2081. https://doi.org/10.1175/1520-0493(1990)118<2056:MWROTN>2.0.CO;2

Vitart, F. (2017). Madden-Julian Oscillation prediction and teleconnections in the S2S database. *Quarterly Journal of the Royal Meteorological Society*, *143*(706), 2210–2220. https://doi.org/10.1002/qj.3079

Wheeler, M. C., & Hendon, H. H. (2004). An all-season real-time multivariate MJO index: Development of an index for monitoring and prediction. *Monthly Weather Review*, *132*(8), 1917–1932. https://doi.org/10.1175/1520-0493(2004)132<1917:AARMMI>2.0.CO;2

Woollings, T., Hannachi, A., & Hoskins, B. (2010). Variability of the North Atlantic eddy-driven jet stream. *Quarterly Journal of the Royal Meteorological Society*, *136*(649), 856–868. https://doi.org/10.1002/qj.625

Woollings, T., Hoskins, B., Blackburn, M., & Berrisford, P. (2008). A new rossby wave–breaking interpretation of the North Atlantic Oscillation. *Journal of the Atmospheric Sciences*, *65*(2), 609–626. https://doi.org/10.1175/2007JAS2347.1

Yadav, P., & Straus, D. M. (2017). Circulation response to fast and slow MJO episodes. *Monthly Weather Review*, *145*(5), 1577–1596. https://doi.org/10.1175/MWR-D-16-0352.1

Zhang, W., Wang, Z., Stuecker, M. F., Turner, A. G., Jin, F. F., & Geng, X. (2018). Impact of ENSO longitudinal position on teleconnections to the NAO. *Climate Dynamics*, *52*(1–2), 257–274. https://doi.org/10.1007/s00382-018-4135-1